ECCOMAS Congress 2016
VII European Congress on Computational Methods in Applied Sciences and Engineering
M. Papadrakakis, V. Papadopoulos, G. Stefanou, V. Plevris (eds.)
Crete Island, Greece, 5–10 June 2016

ANALYSIS OF STOCHASTIC DYNAMIC SOIL-STRUCTURE INTERACTION PROBLEMS BY MEANS OF COUPLED FINITE ELEMENTS-PERFECTLY MATCHED LAYERS

Manthos Papadopoulos, Stijn François, Geert Degrande and Geert Lombaert

KU Leuven, Department of Civil Engineering, Structural Mechanics Section
Kasteelpark Arenberg 40, 3001 Leuven, Belgium
e-mail: {manthos.papadopoulos, stijn.francois, geert.degrande, geert.lombaert}@bwk.kuleuven.be

Keywords: Dynamic soil-structure interaction, stochastic analysis, perfectly matched layers, functionally graded finite elements.

Abstract. *This paper presents a probabilistic computational model for the dynamic soil-structure interaction problem. Specifically, the structure and a limited bounded volume of subsoil in its vicinity are modeled with functionally graded finite elements, allowing to consider heterogeneous local subsoil conditions. This part of subsoil is modeled as a three-dimensional constrained stochastic field. The unboundedness of the surrounding soil is accounted for by coupling the finite element model with perfectly matched layers. An incident wave field is incorporated in the finite element-perfectly matched layers model without explicitly including the source in the computational domain by decomposing the displacement field of the soil in accordance with the subdomain formulation developed for the soil-structure interaction problem. The proposed methodology is illustrated with a case study in which the overall uncertainty is propagated by means of Monte Carlo simulation. The analysis shows that the uncertainty of the structural response increases at specific frequency bands and generally for higher frequencies. These results illustrate how the stochastic variability of the subsoil properties affect both the incident wave field and the structural response in a wide frequency range, and sets the base for future investigations.*

1 INTRODUCTION

Dynamic soil-structure interaction (SSI) refers to the dynamic behavior of the coupled soil-structure system. This problem occurs in several applications from earthquake engineering to the prediction of traffic induced vibrations in the built environment. Pioneering work on the subject started in the nuclear industry for the design and construction of earthquake resistant nuclear reactors. More recently, the development of high-speed railway lines in Europe, east Asia and USA turned research interest also in the field of railway induced vibrations. Railway induced vibrations may lead to malfunctioning of sensitive equipment, discomfort to people and, at high vibration levels, damage to structures. The development of computational models that efficiently and effectively predict the dynamic response of structures excited by ground born vibrations is a matter of ongoing research.

When the knowledge of the subsoil properties is incomplete, the dynamic soil-structure interaction problem should be cast into a stochastic form. This can be done by considering parametric [14] and/or non-parametric uncertainty [3]. Most of the previously conducted work on the subject is mainly focused on earthquake engineering applications considering the very low frequency range (< 10 Hz). The present study considers parametric uncertainty and focuses on the prediction of vibrations in the built environment which makes the frequency range of interest much broader.

The remainder paper is organized as follows. First, the stochastic dynamic soil-structure interaction problem is introduced and the available modeling techniques are briefly discussed. Next, the particularities of modeling the stochastic subsoil are addressed. Finally, the results of a case study are presented, and conclusions are drawn.

2 THE STOCHASTIC DYNAMIC SSI

The soil immediately below the structure plays a dominant role in the structural response. In many cases, this soil is imperfectly known as it may have been perturbed during construction and its characteristics are likely to be different from those identified by geophysical tests on virgin land next to the structure. As discussed in the following, the use of finite elements (FE) provides a great flexibility that allows to incorporate heterogeneous properties in the modeling of this bounded volume of soil. The structure of interest and the limited bounded volume of soil in its vicinity will be denoted for convenience as the generalized structure (Figure 1).

The main difficulty in the modeling of dynamic soil-structure interaction stems from the semi-infinite extent of the soil surrounding the generalized structure, for which the radiation conditions of the elastodynamic waves to infinity should be satisfied. Generally, the dynamic soil-structure interaction problem can be formulated either directly or by following a domain decomposition technique [18]. In the direct approach, the unboundedness of the surrounding soil is accounted for by using appropriate absorbing boundaries in the limits of the regular domain (i.e. generalized structure). The use of perfectly matched layers (PML) [2] is a quite versatile solution to impose these boundary conditions. In the subdomain approach [1], the system is decomposed into two subsystems: the generalized structure and the soil. Both subsystems are analyzed separately and usually by a different computational method. The boundary element method can be used to simulate the unbounded soil domain of infinite extent, where the radiation conditions to infinity are implicitly satisfied, while the finite element method is typically used for the generalized structure.

Although the use of boundary elements entails the benefit of rendering three-dimensional problems in two-dimensional ones, the resulting boundary element system matrices are fully

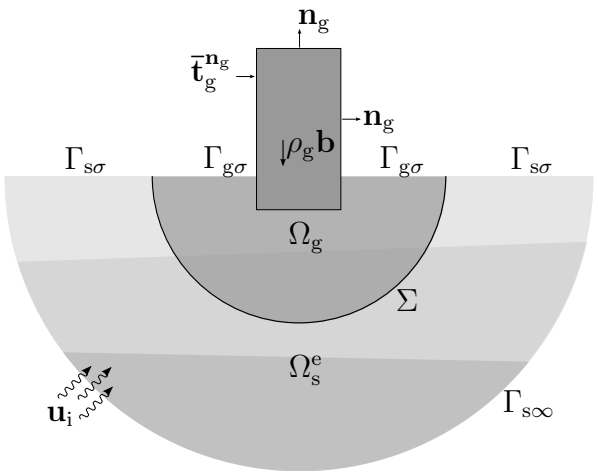

Figure 1: Dynamic soil-structure interaction problem. The interface Σ defines the physical boundary between the unbounded soil $\Omega_\mathrm{s}^\mathrm{e}$ and the generalized structure Ω_g.

populated as opposed to the sparse finite element matrices, leading to increased memory requirements and longer computer time for processing. This aggravates in the case of embedded or extended foundations where a large soil-foundation interface has to be considered. For these reasons, the direct formulation of the problem by means of FE-PML is advocated in this study.

The PML are non-physical absorbing layers that are placed at the exterior limits of the computational domain (Figure 2). Ideally, the waves that are outwardly propagating from the regular domain are fully attenuated inside the PML without any spurious reflections emerging [2]. The effectiveness of the PML strongly depends on the choice and parameterization of their stretch functions [8]. The bounded soil domain is modeled with finite elements: a distinction is made between heterogeneous functionally graded finite elements [13] with continuously varying properties and deterministic homogeneous finite elements. The former are used for the stochastic soil subdomain while the latter are used to enforce the perfectly matched conditions between the PML and the functionally graded FE. The resulting finite element system of equations of the total system is written in the frequency domain as:

$$\hat{\mathbf{K}}\hat{\mathbf{u}} = \hat{\mathbf{f}} \tag{1}$$

where $\hat{\mathbf{f}}$ is the load vector, $\hat{\mathbf{u}}$ is the displacement vector and $\hat{\mathbf{K}}$ is the dynamic stiffness matrix. The dynamic stiffness matrix $\hat{\mathbf{K}}$ can be subdivided into block matrices according to the degrees of freedom: $\hat{\mathbf{u}}_\mathrm{b}$ of the structure, $\hat{\mathbf{u}}_\mathrm{t}$ of the stochastic-heterogeneous soil, $\hat{\mathbf{u}}_\Sigma$ of the interface Σ delimiting the limits of the regular domain, $\hat{\mathbf{u}}_\mathrm{q}$ of the deterministic-homogeneous soil and $\hat{\mathbf{u}}_\mathrm{p}$ the non-physical degrees of freedom of the PML (Figure 2):

$$\begin{bmatrix} \hat{\mathbf{K}}_{\mathrm{bb}} & \hat{\mathbf{K}}_{\mathrm{bt}} & \mathbf{0} & \mathbf{0} & \mathbf{0} \\ \hat{\mathbf{K}}_{\mathrm{tb}} & \hat{\mathbf{K}}_{\mathrm{tt}} & \hat{\mathbf{K}}_{\mathrm{t}\Sigma} & \mathbf{0} & \mathbf{0} \\ \mathbf{0} & \hat{\mathbf{K}}_{\Sigma\mathrm{t}} & \hat{\mathbf{K}}_{\Sigma\Sigma} & \hat{\mathbf{K}}_{\Sigma\mathrm{q}} & \mathbf{0} \\ \mathbf{0} & \mathbf{0} & \hat{\mathbf{K}}_{\mathrm{q}\Sigma} & \hat{\mathbf{K}}_{\mathrm{qq}} & \hat{\mathbf{K}}_{\mathrm{qp}} \\ \mathbf{0} & \mathbf{0} & \mathbf{0} & \hat{\mathbf{K}}_{\mathrm{pq}} & \hat{\mathbf{K}}_{\mathrm{pp}} \end{bmatrix} \begin{bmatrix} \hat{\mathbf{u}}_\mathrm{b} \\ \hat{\mathbf{u}}_\mathrm{t} \\ \hat{\mathbf{u}}_\Sigma \\ \hat{\mathbf{u}}_\mathrm{q} \\ \hat{\mathbf{u}}_\mathrm{p} \end{bmatrix} = \begin{bmatrix} \hat{\mathbf{f}}_\mathrm{b} \\ \hat{\mathbf{f}}_\mathrm{t} \\ \hat{\mathbf{f}}_\Sigma \\ \mathbf{0} \\ \mathbf{0} \end{bmatrix} \tag{2}$$

Excitation sources can be located either close to the receiver like in the case of railway induced vibrations or far from the receiver like in case of an earthquake. If the interest of the analysis is limited only in the neighborhood of the receiver, a remote excitation source S

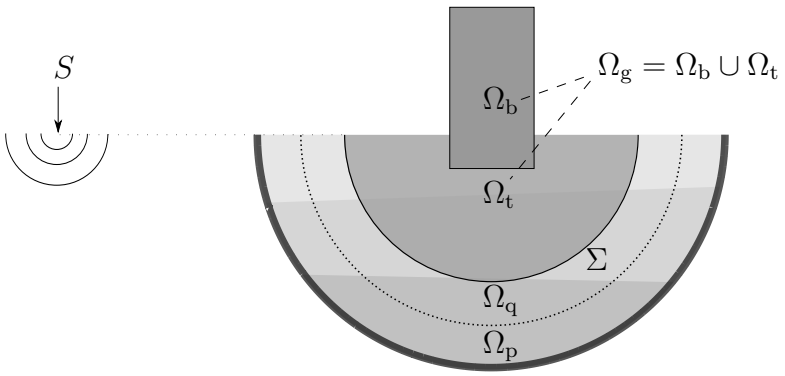

Figure 2: Formulation of the stochastic dynamic soil-structure interaction problem by means of FE-PML. The computational domain is subdivided into the structural Ω_b, stochastic soil Ω_t, deterministc soil Ω_q and PML Ω_p subdomains respectively. All but the last are modeled with finite elements. The interface Σ defines the limits of the regular computational domain.

(Figure 2) can be implicitly taken into account by decomposing the displacement field of the soil in accordance with the subdomain formulation developed for the soil-structure interaction problem [1]. This way, the computational cost decreases significantly as only the generalized structure has to be included in the regular domain. Specifically, the displacement field of the soil is decomposed as (Figure 3):

$$\hat{\mathbf{u}}_s = \hat{\mathbf{u}}_i + \hat{\mathbf{u}}_{d0} + \hat{\mathbf{u}}_d \tag{3}$$

where $\hat{\mathbf{u}}_i$ are the free field displacements generated by the remote source S (Figure 3b). Generally, the free field displacements $\hat{\mathbf{u}}_i$ (and tractions $\hat{\mathbf{t}}_i$) can be computed by using the appropriate source model. The locally diffracted wave field $\hat{\mathbf{u}}_{d0}$ is defined as the displacement field that is radiated in the soil with excavated the generalized structure for which applies $\hat{\mathbf{u}}_{d0} = -\hat{\mathbf{u}}_i$ on the interface Σ (Figure 3c). The wave field $\hat{\mathbf{u}}_d$ corresponds to the displacement field radiated in the soil due to the generalized structure displacements $\hat{\mathbf{u}}_g$ on the interface Σ (Figure 3d). Only the first and the second of the aforementioned displacement fields contribute to the equivalent loading vector $\hat{\mathbf{f}}_\Sigma$ on the interface Σ of the FE-PML model which represents excitation by a remote source.

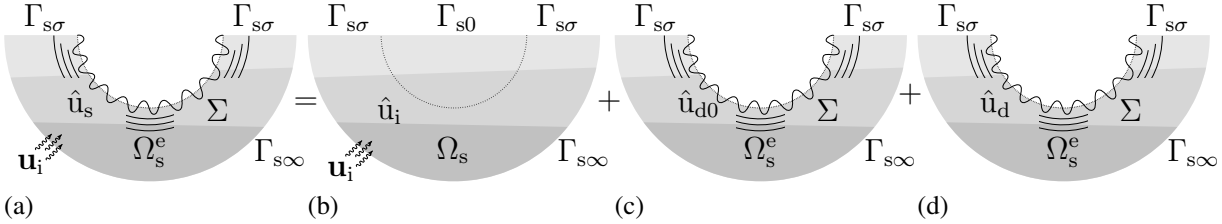

Figure 3: Decomposition of soil displacement field in accordance with the subdomain formulation of the dynamic soil-structure interaction problem. (a) The displacement field in the soil $\hat{\mathbf{u}}_s$ is decomposed into: (b) free field $\hat{\mathbf{u}}_i$, (c) locally diffracted $\hat{\mathbf{u}}_{d0}$ (with $\hat{\mathbf{u}}_{d0} = -\hat{\mathbf{u}}_i$ on Σ) and (d) structurally radiated $\hat{\mathbf{u}}_d$ (with $\hat{\mathbf{u}}_d = \hat{\mathbf{u}}_g$ on Σ).

Once the free field displacements $\hat{\mathbf{u}}_i$ and tractions $\hat{\mathbf{t}}_i$ have been evaluated on the interface Σ, the loading $\hat{\mathbf{f}}_\Sigma$ can be computed as:

$$\hat{\mathbf{f}}_\Sigma = -\int_\Sigma \mathbf{N}_\Sigma^{\mathbf{T}} \hat{\mathbf{t}}_i^{\mathbf{n_s^e}} d\Sigma - \hat{\mathbf{r}}_\Sigma\left(\hat{\mathbf{u}}_{\mathbf{d0}}\right) = -\int_\Sigma \mathbf{N}_\Sigma^{\mathbf{T}} \hat{\mathbf{t}}_i^{\mathbf{n_s^e}} d\Sigma - \hat{\mathbf{r}}_\Sigma\left(-\hat{\mathbf{u}}_{\mathbf{i}}\right) \tag{4}$$

where $\mathbf{N}_\Sigma$ is a matrix containing the shape functions of the finite element faces located on the interface Σ, $\hat{t}_i^{\mathbf{n_s^e}}$ are the free field tractions and $\hat{\mathbf{r}}_{\mathbf{\Sigma}}\left(-\hat{\mathbf{u}}_{\mathbf{i}}\right)$ is a vector of the reaction forces on the interface Σ of the FE-PML model with excavated the generalized structure due to the imposed displacements $-\hat{\mathbf{u}}_{\mathbf{i}}$ (figure 4). The reaction forces $\hat{\mathbf{r}}_{\mathbf{\Sigma}}\left(-\hat{\mathbf{u}}_{\mathbf{i}}\right)$ are computed as follows:

$$\hat{\mathbf{r}}_{\mathbf{\Sigma}}\left(-\hat{\mathbf{u}}_{\mathbf{i}}\right) = \left(\hat{\mathbf{K}}_{\Sigma \mathrm{r}}\hat{\mathbf{K}}_{\mathrm{rr}}^{-1}\hat{\mathbf{K}}_{\mathrm{r}\Sigma} - \hat{\mathbf{K}}_{\Sigma\Sigma}\right)\hat{\mathbf{u}}_{\mathbf{i}} \tag{5}$$

where the degrees of freedom of the deterministic soil $\hat{\mathbf{u}}_{\mathrm{q}}$ and the PML $\hat{\mathbf{u}}_{\mathrm{p}}$ have been grouped for clarity as $\hat{\mathbf{u}}_{\mathrm{r}} = \hat{\mathbf{u}}_{\mathrm{q}} \cup \hat{\mathbf{u}}_{\mathrm{p}}$. The stochastic variation of the soil properties inside the generalized structure does not affect the loading vector $\hat{\mathbf{f}}_\Sigma$ and as a result, in a Monte Carlo analysis it has to be computed only once.

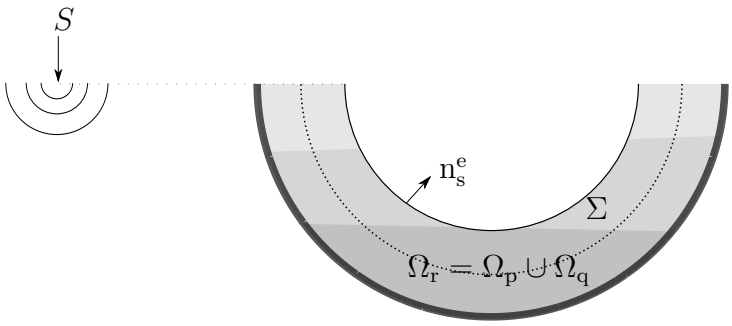

Figure 4: FE-PML model with excavated the stochastic soil subdomain. Auxiliary model for the incorporation of an incident wave field.

3 THE STOCHASTIC SUBSOIL MODELING

The imperfectly known subsoil is modeled as a stochastic field with given marginal probability distribution function (PDF) and correlation structure [17]. Usually, the mean value and the standard deviation are the only available information for the probabilistic characterization of the subsoil properties. In the absence of more detailed experimental results, a covariance function is assumed for the stochastic field. The covariance function is usually defined by the standard deviation function $\sigma_{\mathrm{G}}(s)$ and a correlation structure $\kappa_{\mathrm{G}}(s, s')$:

$$C_{\mathrm{G}}(s, s') = \sigma_{\mathrm{G}}(s)\sigma_{\mathrm{G}}(s')\kappa_{\mathrm{G}}(s, s') \tag{6}$$

This information is sufficient to generate realizations of Gaussian stochastic fields. In this study, non-Gaussian stochastic field realizations are generated by non-linear transformation of the underlying Gaussian. This is referred as translation process [7, 10]:

$$G(\theta, \boldsymbol{s}) = F_{\mathrm{G}}^{-1}\left(F_{\mathrm{Z}}\left(Z(\theta, \boldsymbol{s})\right)\right) \tag{7}$$

where F_{G}^{-1} is the inverse of the target non-Gaussian marginal cumulative probability distribution and Z is the standard normal cumulative probability distribution.

Furthermore, in order to avoid non-physical dynamic impedance contrasts, a conforming coupling between the stochastic and the deterministic subdomains of the soil is desirable. This is achieved by modeling a conditional (or constrained) stochastic field [17]. Conditional stochastic fields are necessarily heterogeneous as the mean value and standard deviation vary from location to location [11].

The Karhunen-Loève expansion can be employed to straightforwardly generate realizations of a heterogeneous Gaussian stochastic field [16]. Nevertheless, the computation of the Karhunen-Loève modes entails the solution of a Fredholm eigenvalue problem [6], which is computationally rather expensive and not trivial to implement in this case. Instead, the approach that is followed in this study is to directly discretize the stochastic field and its covariance matrix into a random vector and a covariance matrix respectively [9]. Subsequently, the random vector describing the Gaussian stochastic field is decorrelated by performing eigenvalue analysis to its covariance matrix:

$$\mathbf{\Lambda} = \mathbf{\Phi}^{\mathbf{T}} \mathbf{C}_{\mathrm{Z}} \mathbf{\Phi} \tag{8}$$

where $\mathbf{\Lambda}$ and $\mathbf{\Phi}$ are matrices containing the eigenvalues λ_{i} and the eigenvectors ϕ_{i} of the covariance matrix $\mathbf{C}_{\mathrm{Z}}$ respectively. The Gaussian realizations are computed as the superposition of the deterministic eigenvectors ϕ_{i} of the covariance matrix multiplied by random numbers ξ_{i} from the standard normal distribution. This corresponds to an equivalent discrete Karhunen-Loève expansion:

$$\mathbf{Z} = \mathbf{Z}_0 + \sum_{i=1}^{n_{\mathrm{m}}} \phi_{\mathrm{i}} Y_{\mathrm{i}} \quad = \mathbf{Z}_0 + \sum_{\mathbf{i}=1}^{\mathbf{n_m}} \phi_{\mathrm{i}} \sqrt{\lambda_{\mathrm{i}}} \xi_{\mathrm{i}} \tag{9}$$

Having generated the Gaussian realizations, the non-Gaussian are generated by following the translation process outlined previously. In Equation 9, the number of eigenvalues considered in the summation should be sufficiently large in order to capture the relevant information that is encoded in the covariance matrix. The first n_{m} largest magnitude eigenvalues, that result in normalized accumulated sum larger than a threshold value ϵ_{min} can be used as a selection criterion:

$$\epsilon(n_{\mathrm{m}}) = \frac{\sum_{i=1}^{n_{\mathrm{m}}} \lambda_i}{\mathrm{tr}(\mathbf{C}_{\mathrm{Z}})} \geq \epsilon_{\mathrm{min}} \tag{10}$$

where $\mathrm{tr}(\mathbf{C}_{\mathrm{Z}})$ is the trace of the covariance matrix.

In a Monte Carlo simulation, when random realizations are generated from the entire sampling space, clusters of realizations may form and as a result the space might not be equally explored. In order to improve the representativeness of the sampled pool of realizations, more sophisticated sampling techniques can be employed. Latin hypercube sampling with artificial correlation reduction is used in the present investigation [12].

4 CASE STUDY

The methodology is illustrated with a case study. A three story R/C office building with regular layout and slab foundation resting at the surface of a visco-elastic halfspace is studied (Figure 5). The characteristics of the building are summarized in Table 1, while the mean properties of the visco-elastic halfspace are shown in Table 2.

Figure 6 shows the FE-PML computational model. The subsoil domain is modeled with three-dimensional twenty-node finite elements. An element size of maximum 2.6 m is used for the mesh at the exterior limits of the computational domain, corresponding to 2.5 quadratic finite elements per shear wavelength λ_s at a frequency of 50 Hz, which is the upper limit considered in this work. The building is modeled with frame and eight-node shell elements. Standard

Story height h_s	3 m
Columns	0.35 m $\times$ 0.35 m
Beams	0.20 m $\times$ 0.50 m
x direction walls	0.20 m $\times$ 4 m
y direction walls	0.20 m $\times$ 2 m
Slab thickness t_s	0.15 m
Raft foundation thickness t_f	0.60 m
Young's modulus E_s	30 GPa
Material density ρ_s	2500 $\mathrm{kg/m^3}$

Table 1: R/C building characteristics.

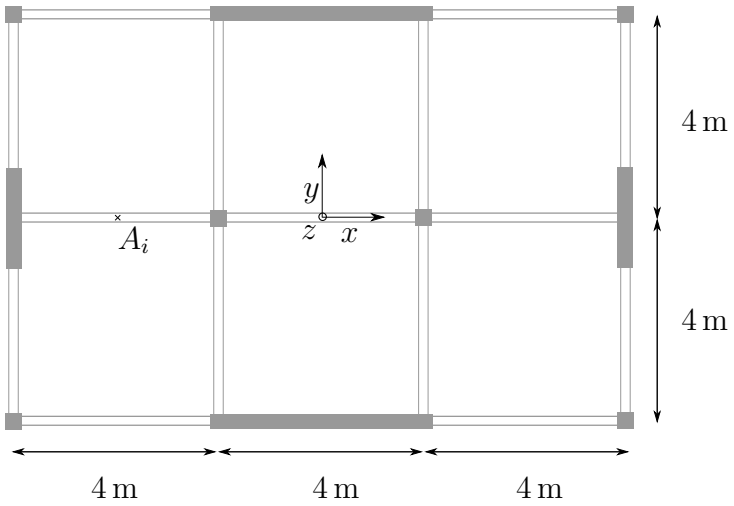

Figure 5: R/C building layout at floor i.

h	C_s	C_p	G	ν	ρ	β
[m]	[m/s]	[m/s]	[MPa]	[$-$]	[kg/m^3]	[$-$]
∞	300	600	162	1/3	1800	0.01

Table 2: Mean properties of the visco-elastic halfspace.

stretch functions are used for the formulation of the PML [8]. Because of the specifically employed FE discretization and PML parameterization, the model is appropiate for analysis in the frequency range between 10 Hz and 50 Hz. As the analysis is performed in the frequency domain, hysteretic damping is assumed for the R/C building with $\eta = 2\xi = 5\%$ [4].

First, the methodology for the incorporation of an incident wave field in the FE-PML model is verified. The homogeneous visco-elastic halfspace with the properties of Table 2 is used for this purpose. The visco-elastic halfspace is excited by a remote source S of unit amplitude located at (-34 m,-26 m,0 m) with respect to the origin of the reference system (Figure 6). The analysis is performed for the computation of the free field displacements without the presence of the R/C building. Figure 7 shows both the solutions obtained with the FE-PML model and the direct stiffness method [15]. The obtained results match perfectly for the frequencies at 10 Hz and 30 Hz, while small differences ($< 5\%$) are observed for the frequency at 50 Hz. This

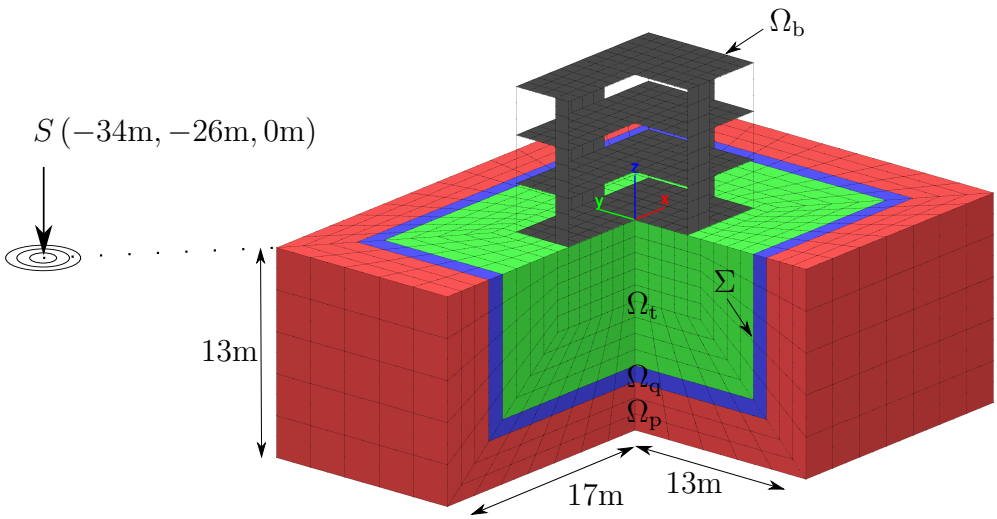

Figure 6: FE-PML model. Regular domain: heterogeneous functionally graded FE (green color) and homogeneous deterministic FE (grey and blue colors). PML domain (red color). Remote excitation source S located outside the limits of the computational domain.

difference can be mostly attributed to discretization error.

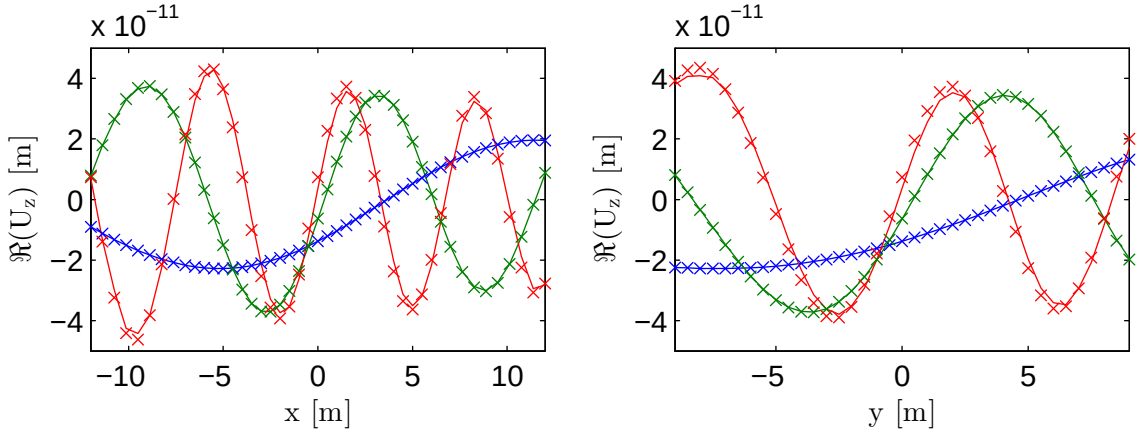

(a) (b)

Figure 7: Real part of vertical free field displacements along the (a) x and (b) y axes (z=0) of the FE-PML model. FE-PML model (solid lines) versus EDT solutions (x marks) [15]. Responses for 10 Hz (blue), 30 Hz (green) and 50 Hz (red).

Next, the R/C building is added at the surface of the stochastic soil. The soil has the mean properties of Table 2 and only the shear modulus is considered to be stochastic. The Gamma PDF is adopted for the shear modulus with a coefficient of variation of $\text{CoV} = 0.3$ (Figure 8). An exponential correlation structure with a correlation length of $l_c = 1.5$ is assumed for the

covariance function of the univariate stochastic field:

$$C_{\mathrm{G}}(s,s') = \sigma_{\mathrm{G}}^2 \exp\left(-\frac{|s-s'|^2}{l_{\mathrm{c}}^2}\right) \tag{11}$$

A threshold value $\epsilon_{\min} = 0.95$ (Equation 9) is used in the present work for the generation of the stochastic field realizations, resulting in $n_{\mathrm{m}} = 1000$ eigenvalues (figure 9). A large number of eigenvalues (and therefore random numbers) is generally required for an adequate representation of weakly correlated stochastic fields. Figure 10 shows a realization of the stochastic shear modulus of the soil mapped onto the finite element mesh. The stochastic shear modulus is constrained to take the deterministic value of the surrounding soil on the interface Σ.

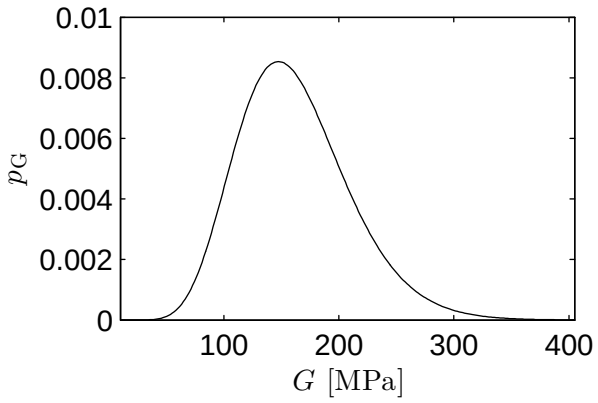

Figure 8: Marginal probability distribution function of soil's shrear modulus.

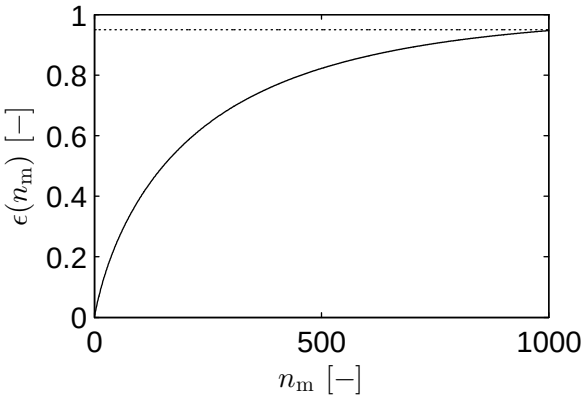

Figure 9: Normalized accumulated sum of Karhunen-Loève eigenvalues.

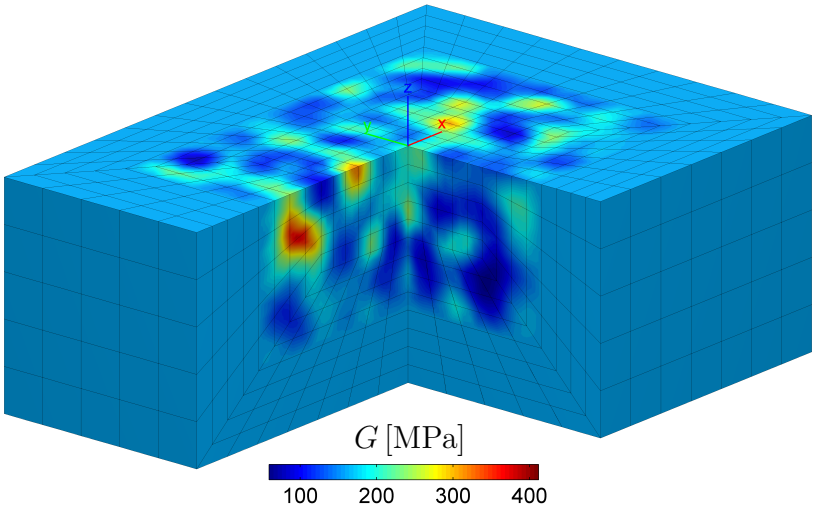

Figure 10: Realization of the stochastic shear modulus of the soil mapped onto the finite element mesh.

The uncertainty is propagated from the stochastic subsoil properties to the structural response quantities by means of Monte Carlo simulation. In total, $n_{\mathrm{R}} = 1001$ realizations are used for the

statistical estimation of the structural response quantities. Moreover, the quality of the estimated statistics is quantified by utilizing the bootstrap method [5]. The degree of uncertainty on the structural response is assessed by means of coefficients of variation and confidence regions. The former are defined as:

$$\mathrm{CoV}_{|\mathrm{U}|} = \frac{\sigma_{|\mathrm{U}|}}{\mu_{|\mathrm{U}|}} \tag{12}$$

where $|U|$ is the modulus of the response quantity U, and $\sigma_{|\mathrm{U}|}$ and $\mu_{|\mathrm{U}|}$ are the standard deviation and the mean value of $|U|$ respectively. Alternatively, a confidence region with a confidence level of $p_c = 90\%$ for the modulus of a response quantity $|U|$ can be defined such that:

$$P(|U_b| \leq |U| \leq |U_t|) \geq p_c \tag{13}$$

where the lower $|U_b|$ and the upper $|U_t|$ bounds can be obtained as the 5% and 95% percentiles of $|U|$ respectively from the Monte Carlo simulation results.

The (stochastic) spatial variability of the subsoil properties affects the structural response in two ways. First, the actual load that excites the structure is altered. Figure 11 shows the free field incident wave field that excites the R/C building in case of homogeneous subsoil conditions, and subsoil conditions as those depicted in Figure 10. Although the same excitation source S (Figure 6) is considered in both cases, the actual free field load that excites the building is different. This happens because, in the latter case, the spatial variability of the subsoil properties, with its inherent subsoil impedance contrasts (Equation 2), may give rise to constructive/destructive inference mechanisms that perturb the incident wave field.

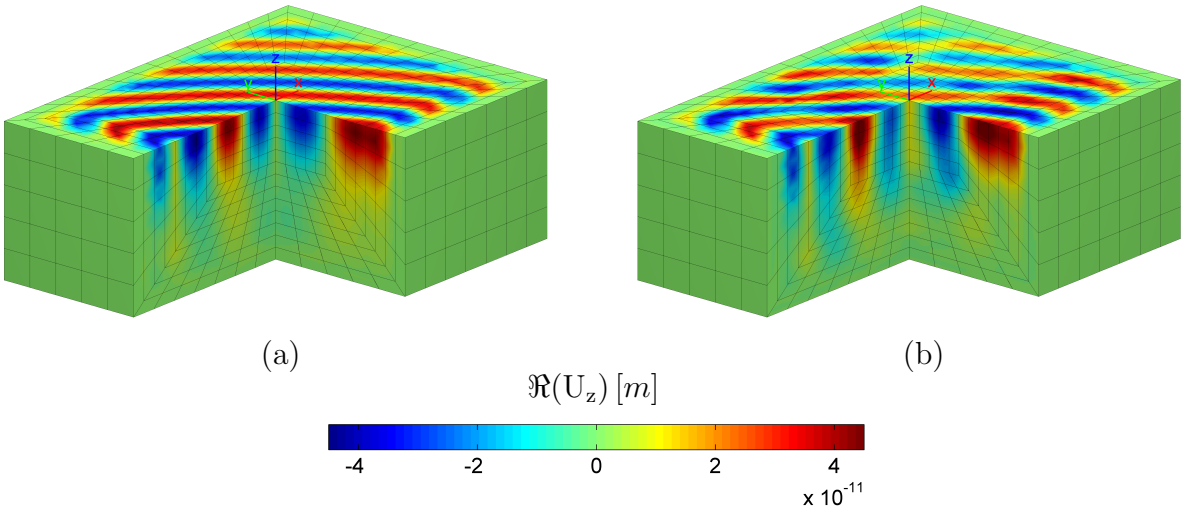

Figure 11: Free field displacements generated by the remote source S at 50 Hz. (a) Homogeneous subsoil conditions and (b) Stochastic realization with heterogeneous subsoil conditions.

Second, the modal characteristics of the coupled structure-soil system are modified. In the case where the loading on the structure is exactly the same for all stochastic subsoil realizations, any difference between the corresponding responses should be solely attributed to the influence that the spatial variability of the subsoil properties has on the modal characteristics of the system. This is demonstrated in Figure 12 which shows the response of node A_1 (Figure 5) in the

y direction in the case where the excitation is directly applied on the R/C building. Specifically, unit amplitude forces are simultaneously imposed on nodes A_1, A_2 and A_3 in the x, y and z directions (the subscripts of A stand for floor number). The mean value of $|U_{\mathrm{y}}|$ is plotted with the corresponding 90% confidence region as function of frequency. The response for five different stochastic subsoil realizations is also plotted. Figure 12b shows the CoV of $|U_{\mathrm{y}}|$ and the corresponding confidence 95% interval for this estimated statistics.

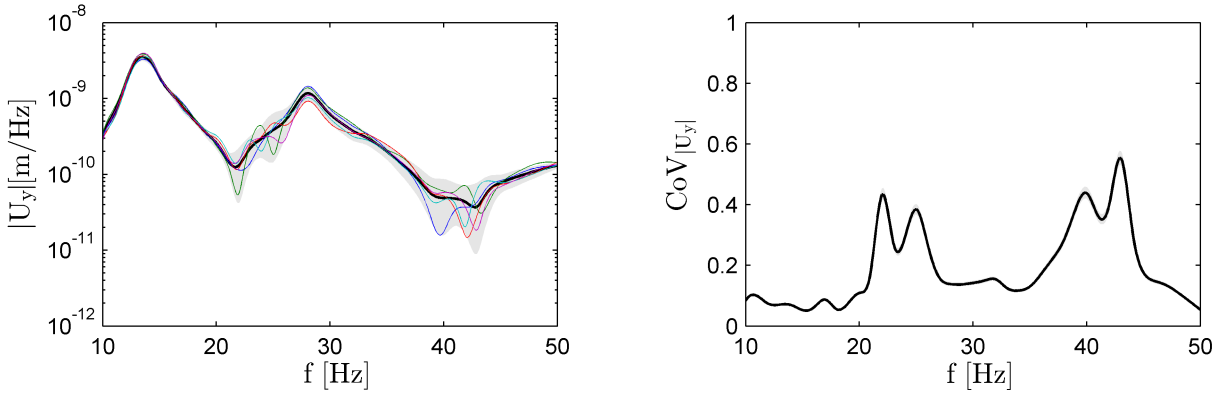

(a) (b)

Figure 12: Modulus of response of node A_1 in the y direction due to applied loading in the x, y and z directions on the nodes A_1, A_2 and A_3. (a) Mean value of response (solid line), the corresponding 90% confidence region of response (shaded area) and five realizations of response (colored lines). (b) Coefficient of variation of response (solid line) and 95% confidence interval for this statistical measure (shaded area).

In case the structure is excited by ground born vibrations, both of the aforementioned effects take place. Figures 13a and 14a show the responses of node A_1 (Figure 5) in the x and z direction, respectively, when the structure is excited by the remote source S (Figure 6). The mean value of $|U_{\mathrm{x}}|$ and $|U_{\mathrm{z}}|$ are plotted with the corresponding 90% confidence regions of response as functions of frequency. Additionally, Figures 13b and 14b show the CoV of $|U_{\mathrm{x}}|$ and $|U_{\mathrm{z}}|$ and the corresponding 95% confidence intervals for these estimated statistics.

A general trend observed in all figures, is that the structural response uncertainty increases at higher frequencies. However, there are certain frequency bands where the response of the coupled soil-structure system is found to be more sensitive to the subsoil properties. Similarly, there are other frequency bands in which the structural response is less sensitive. These frequency bands are not the same for every structural degree of freedom. From the mean response lines (Figures 13a, 14a and 12a), the uncertainty seems to increase at what looks to be the anti-resonance frequencies of the coupled structure-soil system. This can be misleading as these frequencies may correspond to eigenmodes of the coupled soil-structure system which are sensitive to the stochastic subsoil properties. This is demonstrated in Figure 12a, in which individual realization responses are plotted. Frequencies around 24Hz and 40Hz, which seem to be anti-resonance frequencies of the system in the mean response, are actually frequencies where the response of the coupled system is extremely sensitive to the subsoil properties.

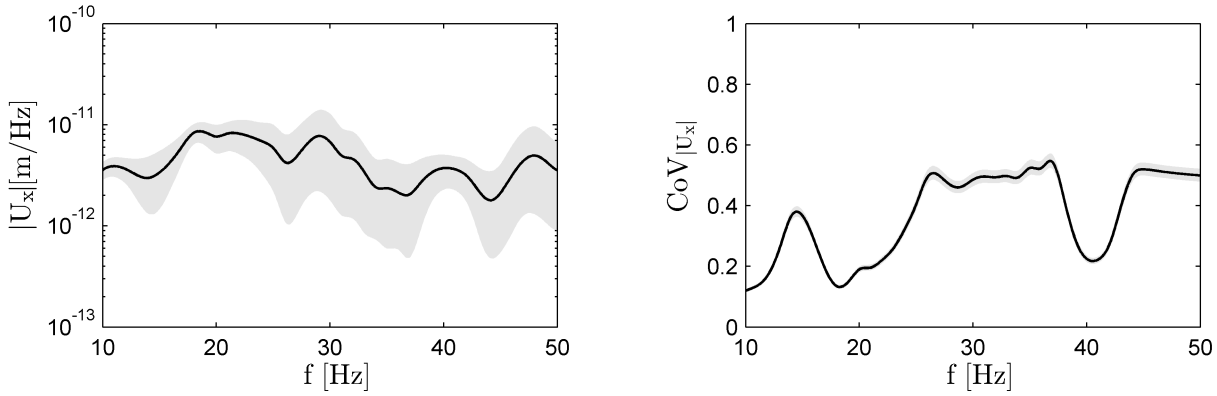

(a) (b)

Figure 13: Modulus of response of node A_1 in the x direction due to excitation by the remote source S. (a) Mean value of response (solid line) and the corresponding 90% confidence region of response (shaded area). (b) Coefficient of variation of response (solid line) and 95% confidence interval for this statistical measure (shaded area).

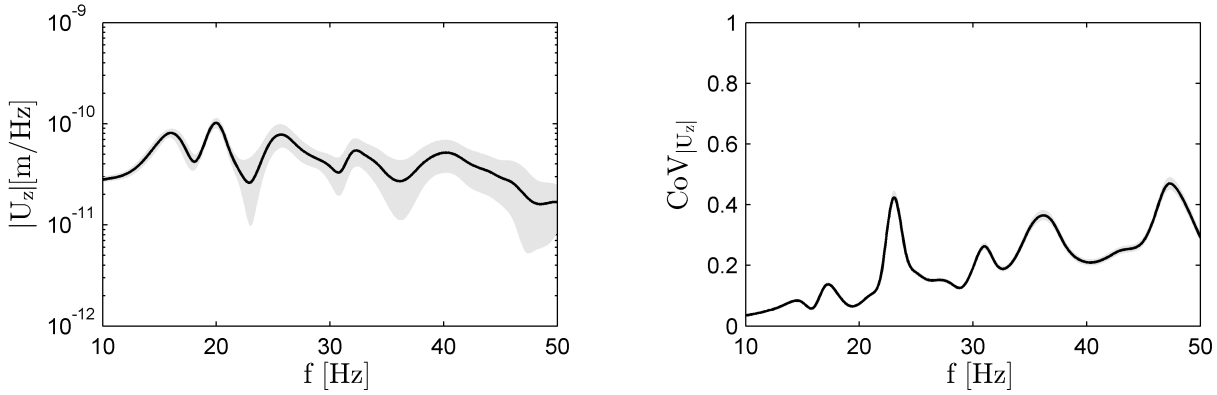

(a) (b)

Figure 14: Modulus of response of node A_1 in the z direction due to excitation by the remote source S. (a) Mean value of response (solid line) and the corresponding 90% confidence region of response (shaded area). (b) Coefficient of variation of response (solid line) and 95% confidence interval for this statistical measure (shaded area).

5 CONCLUSIONS

- A methodology is outlined for the direct formulation of the stochastic soil-structure interaction problem by means of coupled finite elements-perfectly matched layers. The model is suitable for analysis in a wide frequency range.
- The methodology is illustrated with a case study, the results of which set the base for future investigations. The two ways in which the stochastic spatial variability of the subsoil properties affects the structural response are, also, discussed.

- Generally, the structural response uncertainty increases at higher frequencies. However, the structural response sensitivity to the subsoil properties varies considerably over frequency bands.

REFERENCES

[1] D. Aubry, D. Clouteau, A subdomain approach to dynamic soil-structure interaction. In V. Davidovici , R.W. Clough editors, *Recent advances in earthquake engineering and structural dynamics*, p. 251-272, Ouest Editions/AFPS, Nantes, 1992.

[2] U. Basu, A.K. Chopra., Perfectly matched layers for time-harmonic elastodynamics of unbounded domains: theory and finite-element implementation. *Computer Methods in Applied Mechanics and Engineering*, **192(11-12)**, 13371375, 2003.

[3] R. Cottereau, D. Clouteau, C. Soize, S. Cambier Probabilistic nonparametric model of impedance matrices. Application to the seismic design of a structure. *European Journal of Computational Mechanics*, **15**, 131-142, 2006.

[4] R.W. Clough, J. Penzien, *Dynamics of structures*. Computers & Structures Inc., 2003.

[5] B. Efron, R. J. Tibshirani, *An Introduction to the Bootstrap*. Chapman & Hall, 1993.

[6] R.G. Ghanem, P.D. Spanos, *Stochastic Finite Elements: A Spectral Approach*. Springer-Verlag New York, 1991.

[7] M. Grigoriu, Crossings of non-Gaussian translation processes. *Journal of Engineering Mechanics*, **110(4)**, 610-620, 1984.

[8] S. Kucukcoban, L.F. Kallivokas, A symmetric hybrid formulation for transient wave simulations in PML-truncated heterogeneous media. *Wave Motion*, **50**, 57-79, 2013.

[9] C.C. Li, A. Der Kiureghian, Optimal discretization of random fields. *Journal of Engineering Mechanics*, **19(6)**, 11361154, 2003.

[10] P. Liu, A. Der Kiureghian, Multivariate distribution models with prescribed marginals and covariances. *Probabilistic Engineering Mechanics*, **1(2)**, 105-112, 1986.

[11] R.P Nordgren, J.P. Conte, On one-dimensional random fields with fixed end values. *Probabilistic Engineering Mechanics*, **14**, 301-310, 1999.

[12] A. M. J. Olsson, G. E. Sandberg, Latin hypercube sampling for stochastic finite element analysis. *Journal of Engineering Mechanics*, **128:(1)**, 121-125, 2002.

[13] M.H. Santare, P. Thamburaj, G.A. Gazonas, The use of graded finite elements in the study of elastic wave propagation in continuously nonhomogeneous materials. *International Journal of Solids and Structures*, **40**, 5621-5634, 2003.

[14] E. Savin, D. Clouteau, Elastic wave propagation in a 3D unbounded random heterogeneous medium coupled with a bounded medium. Application to seismic soilstructure interaction (SSSI). *International Journal for Numerical Methods in Engineering*, **54**, 607-630, 2002.

[15] M. Schevenels, G. Degrande, S. Francois, EDT: An ElastoDynamics Toolbox for MATLAB. *Computers & Geosciences*. In press. http://dx.doi.org/10.1016/j.cageo.2008.10.012

[16] G. Stefanou, The stochastic finite element method: Past, present and future. *Computational Methods in Applied Mechanics and Engineering*, **198**, 1031-1051, 2009.

[17] E. Vanmarcke, *Random Fields: Analysis and Synthesis*. MIT Press Classics, 1983.

[18] J.P. Wolf, *Dynamic soil-structure interaction*. Prentice-Hall, 1985.